JOC Article

Synthesis, Spectroscopy, and Theoretical Calculations for a Series of Push−Pull [14]-Pyridoannulenes

Matthew G. Lauer, James W. Leslie, Ashley Mynar, Shelly A. Stamper, Anthony D. Martinez, Adrian J. Bray, Senai Negassi, Kevin McDonald, Eric Ferraris, Aaron Muzny, Shawn McAvoy, Christopher P. Miller, Keith A. Walters,* and Keith C. Russell*

Northern Kentucky University, Department of Chemistry, Highland Heights, Kentucky 41099-1905

Evan Wang, Betsy Nuez, and Carol Parish*

University of Richmond, Department of Chemistry, 28 Westhampton Way, Richmond, Virginia 23173

russellk@nku.edu; walterske@nku.edu; cparish@richmond.edu

Received September 7, 2007

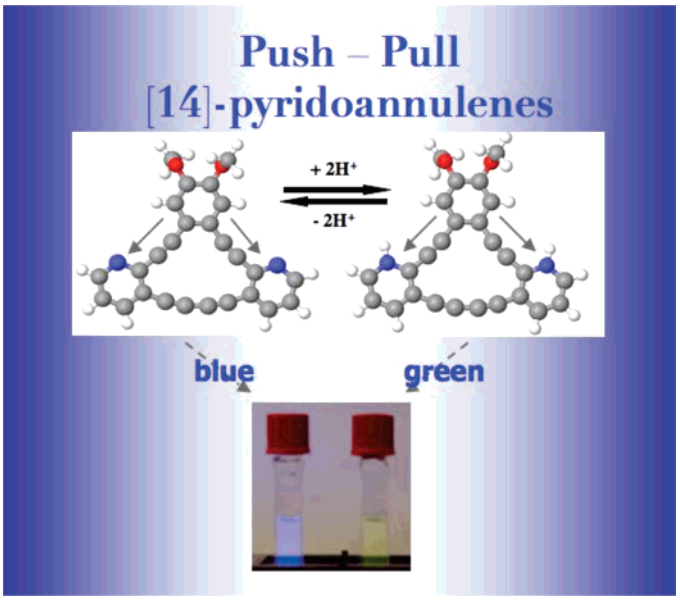

Three new isomeric dipyridoannulenes were synthesized and characterized. These molecules possess differing conjugation pathways between the substituent alkoxy donating groups and the pyridyl acceptor groups. Optical absorption and emission properties of the dipyridoannulenes and their corresponding acyclic precursors were measured and correlated to structural differences and used to evaluate conjugation effectiveness and charge-transfer pathways. Optical properties of protonated dipyridoannulenes were also measured and found to be somewhat insensitive to the degree of protonation. Density functional studies of these systems at the B3LYP/6-31G* level provided insight into their stabilities, polarities, and quinoidal character. An analysis of the HOMO and LUMO molecular orbitals provided further information regarding charge-transfer behavior. These systems are good metal binding candidates, as the pyridine moiety can act as both an electron-acceptor and a site for metal coordination.

Introduction

Cyclic structures composed exclusively of arenes and arenes bridged by unsaturated linkers, dehydrobenzoannulenes (DBAs), have been known for many years.[1] In particular, *o*-DBAs, DBAs where benzene or substituted benzene rings are connected via

* Corresponding author. Fax: (K.C.R.) (859) 572-5162.

(1) Balaban, A. T. *Annulenes: Benzo-, Hetero-, Homo-Derivatives, and Their Valence Isomers, Vols. 1−3*; CRC Press: Boca Raton, FL, 1987.

10.1021/jo7019724 CCC: $40.75
Published on Web 12/18/2007

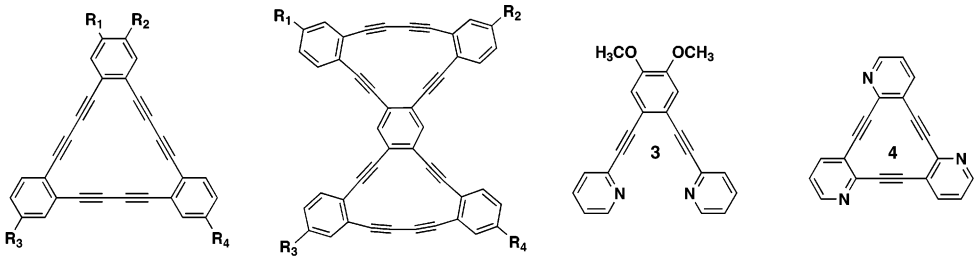

FIGURE 1. Annulenes and related donor−acceptor systems.

the o-position by (poly)alkynyl spacers, have been attractive targets (Figure 1). In large part, this can be attributed to the synthetic accessibility of such molecules via highly reliable palladium coupling strategies.[2] Unmodified *o*-DBAs have been prepared to model graphyne substructures,[3] to be used as precursors to carbon tubes and onions,[4] to examine molecular strain,[5,6] and to study aromaticity.[7] Cyclophane derived *o*-DBA hybrids have been used to probe aromaticity in the annulene framework,[8] while pyrene hybrids have also been used to examine photoisomerism.[9] An *o*-DBA bearing a crown ether was examined for supramolecular assemblage.[10]

More recently, investigators have begun to focus on annulenes and related compounds with pendant electron-donors and -acceptors. Haley's group has extensively examined [18]-annulenes bearing either alkoxy or dialkylamino electron-donors and nitro electron-acceptors (e.g., **1a**−**c**).[11] These compounds were shown to exhibit second-order NLO properties.[12] Later, this same group explored a series of bis-[14-]- and -[15]-annulenes (e.g., **2a**−**c**) and compared them to their acyclic precursors.[13] The results clearly demonstrated that conjugation effectiveness, electron density, planarity, and geometry of charge-transfer pathways profoundly affect the optical properties, stability, and aggregation propensity of DBAs. One disadvantage of these prior systems is that they are generally inappropriate for metal binding. The amino groups, which might be able to interact with metals through their lone pairs, are the electron donors and thus are partially positively charged, while the electron-accepting nitro groups are considered poor ligands in general.

There are now several examples of *o*-DBAs possessing heterocycles such as thiophene[14] or phthalocyanines in the place of some or all of the carbocyclic arenes.[15] The inclusion of heterocycles as part of the annulene allows for metal binding, although it is possible for small [12]-*o*-DBAs to bind metals such as Ni(0) within the central cavity by simultaneous coordination to all of the triple bonds.[16] Many of these compounds have been prepared with the aim of developing new sensors.

More recently, reports have begun to surface where pyridine rings are being used to replace the electron-accepting nitrobenzene in similar structures, simultaneously providing an electron-acceptor and a site for metal coordination. Bunz's group has released a series of papers on **3**, which was shown to behave as a bidentate ligand for appropriate metal cations and whose absorption spectrum was shown to be highly sensitive to acid.[17−19] The only pyridine possessing DBA reported to date is a C_3 symmetric [12]-annulene (**4**) and a related but highly strained twistophane.[20] Annulene **4** was shown to undergo significant spectral changes in the presence of small amounts Pd(II) and acid while the twistophane was sensitive to Hg(II) in addition to Pd(II). A series of cruciform-type structures with pyridine electron-acceptors has also recently been reported.[21] Here, we wish to report our entry into this area with the synthesis and characterization of a series of three new donor−acceptor [14]-dehydropyridoannulenes (**5**−**7**).

These new compounds have interesting conjugation paths. Previous studies on alkyne-containing structures have demonstrated the influence that the conjugation path can have on electronic structure.[22−24] As seen in resonance contributor **5a** (Figure 2), **5** has a bent conjugation route (a) from the oxygen on the right to the nitrogen on the right via an intervening arene and three triple bonds. Likewise, the left oxygen and nitrogen

(2) Marsden, J. A.; Palmer, G. J.; Haley, M. M. *Eur. J. Org. Chem.* **2003**, 2355−2369.
(3) Kehoe, J. M.; Kiley, J. H.; English, J. J.; Johnson, C. A.; Petersen, R. C.; Haley, M. M. *Org. Lett.* **2000**, *2*, 969−972.
(4) Boese, R.; Matzger, A. J.; Vollhardt, K. P. C. *J. Am. Chem. Soc.* **1997**, *119*, 2052−2053.
(5) Tobe, Y.; Ohki, I.; Sonoda, M.; Niino, H.; Sato, T.; Wakabayashi, T. *J. Am. Chem. Soc.* **2003**, *125*, 5614−5615.
(6) Boydston, A. J.; Laskoski, M.; Bunz, U. H. F.; Haley, M. M. *Synlett* **2002**, 981−983.
(7) Matzger, A. J.; Peter, K.; Volhardt, C. *Tetrahedron Lett.* **1998**, *39*, 6791−6794.
(8) Hinrichs, H.; Fischer, A. K.; Jones, P. G.; Hopf, H.; Haley, M. M. *Org. Lett.* **2005**, *7*, 3793−3795.
(9) Kimball, D. B.; Haley, M. M.; Mitchell, R. H.; Ward, T. R.; Bandyopadhyay, S.; Williams, R. V.; Armantrout, J. R. *J. Org. Chem.* **2002**, *67*, 8798−8811.
(10) Pak, J. J.; Weakley, T. J. R.; Haley, M. M.; Lau, D. Y. K.; Stoddart, J. F. *Synthesis* **2002**, 1256−1260.
(11) Pak, J. J.; Weakley, T. J. R.; Haley, M. M. *J. Am. Chem. Soc.* **1999**, *121*, 8182−8192.
(12) Sarkar, S. A.; Pak, J. J.; Rayfield, G. W.; Haley, M. M. *J. Mater. Chem.* **2001**, *11*, 2943−2945.
(13) Marsden, J. A.; Miller, J. J.; Shirtcliff, L. D.; Haley, M. M. *J. Am. Chem. Soc.* **2005**, *127*, 2464−2476.
(14) Sarkar, A.; Haley, M. M. *Chem. Commun.* **2000**, 1733−1734.
(15) Cook, M. J.; Heeney, M. J. *Chem.—Eur. J.* **2000**, *6*, 3958−3967.
(16) Zhang, D. M.; Tessier, C. A.; Youngs, W. J. *Chem. Mater.* **1999**, *11*, 3050−3057.
(17) Shotwell, S.; Windscheif, P. M.; Smith, M. D.; Bunz, U. H. F. *Org. Lett.* **2004**, *6*, 4151−4154.
(18) Shotwell, S.; Ricks, H. L.; Morton, J. G. M.; Laskoski, M.; Fiscus, J.; Smith, M. D.; Shimizu, K. D.; zur Loye, H.-C.; Bunz, U. H. F. *J. Organomet. Chem.* **2003**, *671*, 43−51.
(19) Fiscus, J. E.; Shotwell, S.; Layland, R. C.; Smith, M. D.; zur Loye, H.-C.; Bunz, U. H. F. *Chem. Commun.* **2001**, 2674−2675.
(20) Baxter, P. N. W. *Chem.—Eur. J.* **2003**, *9*, 2531−2541.
(21) Spitler, E. L.; Shirtcliff, L. D.; Haley, M. M. *J. Org. Chem.* **2007**, *72*, 86−96.
(22) Pan, Y.; Lu, M.; Peng, Z.; Melinger, J. S. *J. Org. Chem.* **2003**, *68*, 6952−6958.
(23) Peng, Z.; Pan, Y.; Xu, B.; Zhang, J. *J. Am. Chem. Soc.* **2000**, *122*, 6619−6623.
(24) Nierengarten, J. F.; Zhang, S.; Gegout, A.; Urbani, M.; Armaroli, N.; Marconi, G.; Rio, Y. *J. Org. Chem.* **2005**, *70*, 7550−7557.

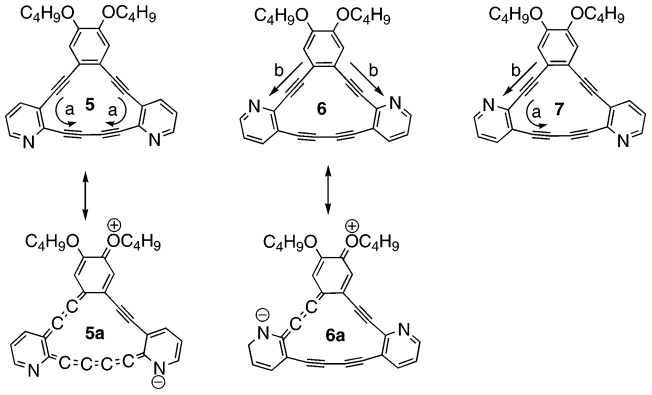

FIGURE 2. Conjugation paths in annulenes **5**−**7**.

SCHEME 1[a]

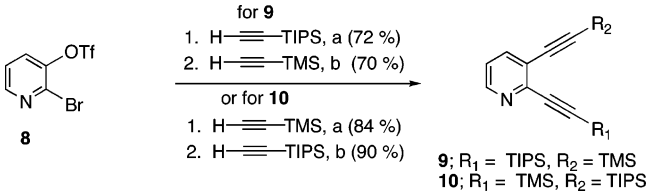

[a] Reagents and conditions: (a) 1.3 equiv of alkyne, $Pd(PhCN)_2Cl_2$, CuI, $[(t\text{Bu})_3\text{PH}]BF_4$, $i\text{Pr}_2\text{NH}$, 58−65 °C, 2 days and (b) 1.5 equiv of alkyne, $Pd(Ph_3P)_4$, $i\text{Pr}_2\text{NH}$, 120 °C, overnight.

have a bent conjugation path. According to prior literature, any cross-conjugation (i.e., right oxygen to left nitrogen or left oxygen to right nitrogen of **5**) is expected to be insignificant.[11] In the case of **6**, there is a shorter, linear conjugation route (b in Figure 2) between the oxygen on the right and the nitrogen on the left that only goes through a single acetylene spacer. This can be visualized by resonance contributor **6a**. The nitrogen on the right is also in resonance with the oxygen on the left. In unsymmetrical annulene **7**, however, the oxygen on the right has conjugation paths to both nitrogens, while only cross-conjugation is available to the oxygen on the left to either nitrogen. Since the final step of the synthesis is the closure of the annulene by formation of the butadiyne bridge, the penultimate precursors will provide excellent information about the role of bent conjugation paths.

Results and Discussion

Synthesis. The synthesis of the annulenes used a convergent strategy using three key building blocks. Pyridinate **8**[25] was used to prepare two differentially protected bis-alkynylpyridine isomers, **9** and **10** (Scheme 1). Sequential Sonogashira coupling of triisopropylsilyl-acetylene (TIPSA) and TMS-acetylene (TMSA) afforded **9** in 71% overall yield for the two steps. Compound **10** was prepared in 70% yield from triflate **8** by switching the order in which the protected alkynes were coupled. This compound has been previously reported by Baxter and Dali-Youcef starting from 2,3-dibromopyridine.[26] The regiospecificity for the first coupling reaction was established by examination of the proton-decoupled ^{13}C NMR spectra of the mono-coupled intermediates. In both cases, the mono-coupled intermediates showed a quartet (F−C splitting) consistent with the presence of the triflate group, providing conclusive evidence that the bromide is selectively replaced. Oddly, all attempts to prepare **9** and **10** from 2,3-dichloropyridine failed. Independent of conditions, it was not possible to achieve good selectivity with respect to the first coupling reaction. In each case, a mixture of starting material and mono- and di-substituted products was obtained.

Annulene **5** was prepared as shown in Scheme 2. The TMS group was selectively removed from **9** in 93% yield. Two equivalents of terminal alkyne **11** was then coupled to 1,2-dibutoxy-4,5-diodobenzene (**12**), yielding donor−acceptor functionalized **13**. Removal of the TIPS groups was achieved with tetrabutylammonium fluoride (TBAF), and the terminal alkynes oxidatively coupled to afford the desired annulene using the procedure reported by Haley et al.[27]

Isomeric annulene **6**, which bears the pyridyl nitrogens facing away from each other, was prepared in a similar fashion from **10** (Scheme 3). Again, the TMS group was selectively removed from **10** in high yield. Two equivalents of alkyne **15** were then coupled to **12** to give rise to **16**. TBAF was used to remove the TIPS groups, and the compound cyclized to yield annulene **6**.

The unsymmetrical annulene isomer, **7**, was prepared as shown in Scheme 4. Equal molar amounts of **15** and **12** were reacted to afford **18** in reasonable yield along with small amounts of **16**. It was not possible to purify **18** completely due to the presence of a coeluting impurity postulated to be a product of the oxidative homocoupling of **15**. When partially purified **18** was coupled with **11**, the unsymmetrical annulene precursor **19** was readily isolated by column chromatography. The TIPS-protected alkynes were liberated, and the free alkynes cyclized as before to render annulene **7**.

NMR Spectra. Figure 3 shows the aromatic region of the ^1H NMR spectra for annulenes **5**−**7**. The assignments for symmetric annulenes **5** and **6** allow for facile determination of the protons in **7**.

Comparison of chemical shift differences between [14]-dehydrobenzoannulenes and their precursors has been frequently used as a probe of aromaticity.[8,9,28,29] These studies have clearly demonstrated that the alkene protons are more sensitive to effects of cyclization than are any arene protons. However, upon cyclization from their precursors, arene protons of dehydrobenzoannulenes generally experience a downfield chemical shift. Likewise, the protons in **5**−**7** and their precursors experience similar chemical shift differences upon cyclization (Table 1). The most sensitive protons are those adjacent to the single alkyne bridges, rather than the butadiyne bridge. The analysis of Hb is interesting. This proton shows a shift difference of 0.45 ppm in the **13** → **5** cyclization. However, in the conversion of **19** to **7**, the difference in chemical shift for this proton is only 0.03 ppm. All other protons show nearly the same chemical shift differential when comparing symmetric annulene **5** and **6** to unsymmetric annulene **7**. The explanation for this might be rationalized by examination of the resonance paths available to the precursors as well as the annulenes. In the case of precursor **13**, only cross-conjugation paths are available between oxygens and nitrogens. After cyclization to annulene **5**, the bent conjugation path through the butadiyne bridge becomes available. This is the only path of direct conjugation

(25) Kim, C.-S.; Russell, K. C. *J. Org. Chem.* **1998**, *63*, 8229−8234.
(26) Baxter, P. N. W.; Dali-Youcef, R. *J. Org. Chem.* **2005**, *70*, 4935−4953.
(27) Marsden, J. A.; Miller, J. J.; Haley, M. M. *Angew. Chem., Int. Ed.* **2004**, *43*, 1694−1697.
(28) Baldwin, K. P.; Matzger, A. J.; Scheiman, D. A.; Tessier, C. A.; Vollhardt, K. P. C.; Youngs, W. J. *Synlett* **1995**, 1215−18.
(29) Boydston, A. J.; Haley, M. M. *Org. Lett.* **2001**, *3*, 3599−3601.

SCHEME 2[a]

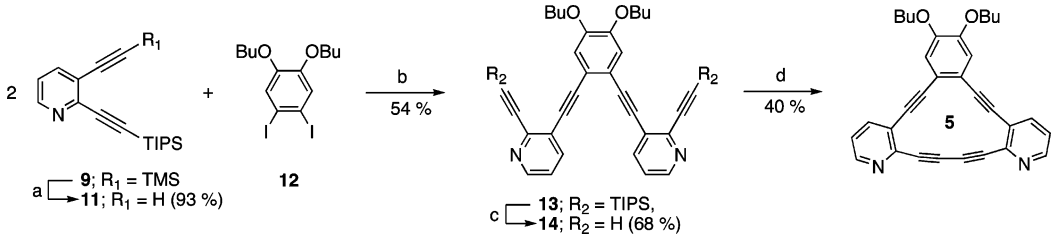

[a] Reagents and conditions: (a) K_2CO_3, CH_3OH, rt, 24 h; (b) $Pd(Ph_3P)_2Cl_2$, CuI, *i*Pr_2NH, 80 °C, 3 days; (c) TBAF, −78 °C to rt, 1 h; and (d) $Pd(dppe)Cl_2$, CuI, I_2, THF, *i*$PrNH_2$, 60 °C, 28 h (14% from **9**).

SCHEME 3[a]

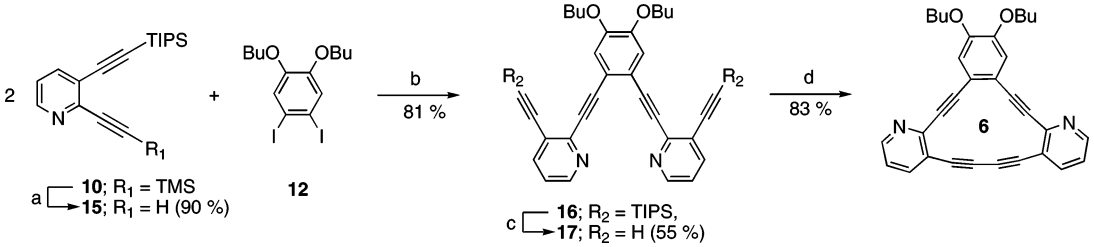

[a] Reagents and conditions: (a) K_2CO_3, CH_3OH, rt, 24 h; (b) $Pd(Ph_3P)_2Cl_2$, CuI, *i*Pr_2NH, 80 °C, 3 days; (c) TBAF, −78 °C to rt, 1 h; and (d) $Pd(dppe)Cl_2$, CuI, I_2, THF, *i*$PrNH_2$, 60 °C, 28 h (33% from **10**).

SCHEME 4[a]

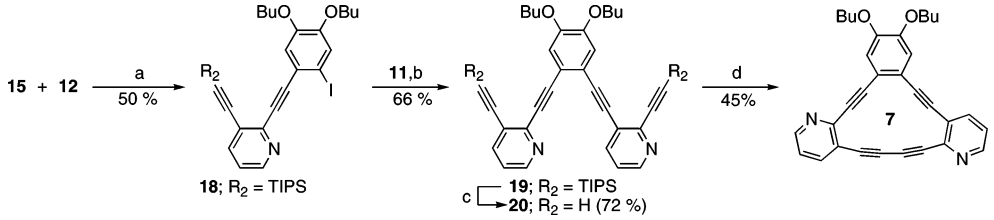

[a] Reagents and conditions: (a) $Pd(Ph_3P)_2Cl_2$, CuI, *i*Pr_2NH, rt, 2 days; (b) $Pd(Ph_3P)_2Cl_2$, CuI, *i*Pr_2NH, 80 °C, 3 days; (c) TBAF, −78 °C to rt, 1 h; and (d) $Pd(dppe)Cl_2$, CuI, I_2, THF, *i*$PrNH_2$, 60 °C, 28 h (11% from **15**).

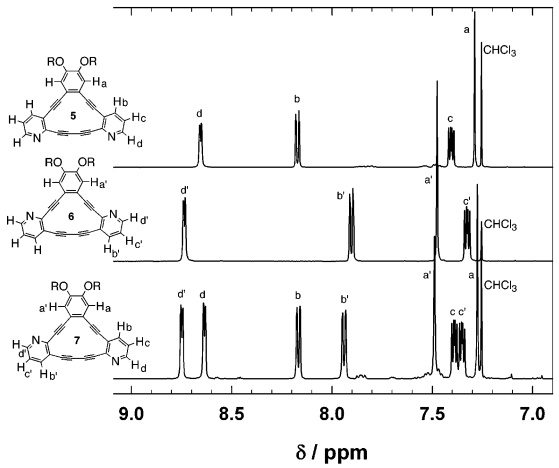

FIGURE 3. ^1H NMR spectra for the aromatic region of annulenes **5**−**7**.

between both oxygens and nitrogens. In the case of precursor **19**, the linear conjugation path is available to the right oxygen/left nitrogen pair, while cross-conjugation is the only route available to the right nitrogen. Once converted to annulene **7**, the bent conjugation path is also possible for the right nitrogen. However, the shorter, linear conjugation route is dominant due to a smaller charge separation. Thus, the cyclization has little effect on proton Hb.

TABLE 1. Chemical Shift Difference of Arene Protons upon Cyclization

	Δδ (ppm)			
proton	**13** → **5**	**16** → **6**	**19** → **7**	Δ(Δδ)[a]
a	0.32		0.29	0.03
b	0.45		0.03	0.42
c	0.29		0.2	0.09
d	0.18		0.19	−0.01
a′		0.44	0.44	0.00
b′		0.15	0.15	0.00
c′		0.18	0.23	−0.05
d′		0.22	0.22	0.00

[a] For a−d = (**13** → **5**) − (**19** → **7**) and for a′−d′ = (**16** → **6**) − (**19** → **7**).

Computational Studies. Simplified compounds **5′**−**7′**, the methyl analogues of **5**−**7**, were used for computational analysis (Figure 4). The structures of **5′**−**7′** were obtained by geometry optimization, without symmetry constraints, using the B3LYP density functional with the 6-31G* basis set as implemented in the Gaussian 03[30] program. The B3LYP/6-31G* treatment has been shown to adequately describe similar systems.[13] Harmonic frequency analysis was used to confirm all structures as

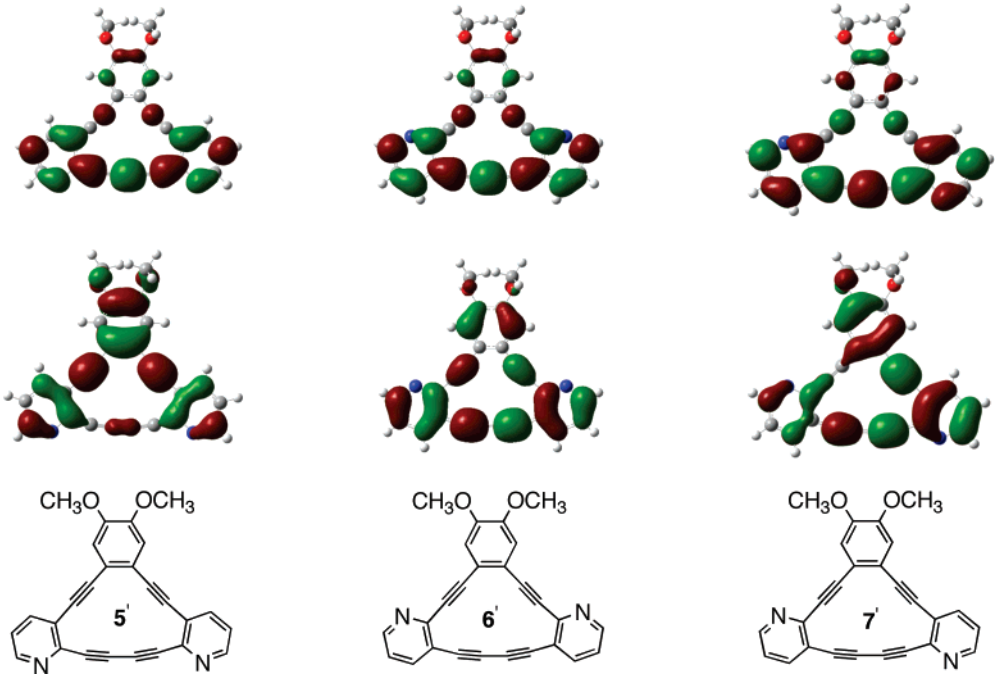

FIGURE 4. Molecular orbital images of **5′**−**7′**. Upper and lower plots are the LUMO and HOMO, respectively.

stationary points on the respective potential energy surface. As expected, the conjugated backbones of **5′**−**7′** are planar with the methoxy groups oriented trans above and below the plane. Calculated bond lengths are provided in Table 2. Bond length alternation can yield insight regarding the aromaticity present in these systems as well as the nature of charge transfer between donor and acceptor moieties. Quinoidal character (δr; eq 1) is a measure often used to describe bond length alternation and the corresponding degree of charge transfer present along conjugated hydrocarbon backbones.[31,32] For calibration, the δr value in benzene is 0, while fully quinoidal rings have values between 0.08 and 0.10. Quinoidal values for pyridine and diethynyl pyridine, calculated at the B3LYP/6-31G* level of theory, are 0.0145 and 0.0223, respectively.

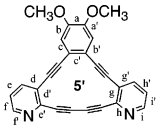

$$\delta r = \frac{\left[\left(a+a'\right)/2-\left(b+b'\right)/2\right]+\left[\left(c+c'\right)/2-\left(b+b'\right)/2\right]}{2} \quad \text{Eqn 1}$$

The quinoidal behavior is similar for **5′**−**7′**; δr values in the donor substituted rings are small, indicating a small degree of quinoidial character, while the δr values in the acceptor rings range from 0.0229 to 0.0253, similar in range to quinoidal values reported for donor−acceptor substituted diphenylacetylene,[31] tetrakis(phenylethynyl)benzenes, and bis(dehydrobenzoannuleno)benzenes.[13] Interestingly, the quinoidal character of the pyridine rings in **5′** is larger (0.0253) than in **6′** (0.0231), perhaps indicating better charge transfer in this system. Molecule **7′**, with nitrogen atoms on opposite sides of the diacteylene bridge, shows a slightly larger quinoidal character for the pyridine ring with the N pointed away from the donor group (0.0253) than for the pyridine group pointed toward the donor group (0.0229).

TABLE 2. Calculated Bond Lengths and Quinoidal Character (δr) of 5′−7′

	Donor						quinoid character
	a	a′	b	b′	c	c′	δr (a−c)
5′	1.4130	1.3871	1.3871	1.4124	1.4124	1.4255	0.0098
6′	1.4132	1.3874	1.3874	1.4120	1.4120	1.4251	0.0097
7′	1.4130	1.3872	1.3874	1.4123	1.4120	1.4252	0.0095

	acceptor						
	d	d′	e	e′	f	f′	δr (d−f)
5′	1.4082	1.4302	1.3869	1.3477	1.4008	1.3311	0.0253
6′	1.3492	1.4311	1.3320	1.4057	1.4005	1.3869	0.0231
7′	1.4082	1.4303	1.3869	1.3478	1.4007	1.3313	0.0252
	g	g′	h	h′	i	i′	δr (g−i)
5′	1.4302	1.4082	1.3477	1.3869	1.3311	1.4008	0.0253
6′	1.4311	1.3492	1.4057	1.3320	1.3869	1.4005	0.0231
7′	1.4307	1.3492	1.4058	1.3320	1.3869	1.4006	0.0229

The B3LYP/6-31G* energetics are shown in the Supporting Information. Energetically, **6′** is the most stable, while **5′** is the least stable, although all systems are within 0.7 kcal/mol of being isoenergetic. Polarity is inversely proportional to stability; **6′** is the least polar, while **5′** has a large dipole moment (6.8241 D).

(30) Frisch, M. J.; Trucks, G. W.; Schlegel, H. B.; Scuseria, G. E.; Robb, M. A.; Cheeseman, J. R.; Montgomery, J. A., Jr.; Vreven, T.; Kudin, K. N.; Burant, J. C.; Millam, J. M.; Iyengar, S. S.; Tomasi, J.; Barone, V.; Mennucci, B.; Cossi, M.; Scalmani, G.; Rega, N.; Petersson, G. A.; Nakatsuji, H.; Hada, M.; Ehara, M.; Toyota, K.; Fukuda, R.; Hasegawa, J.; Ishida, M.; Nakajima, T.; Honda, Y.; Kitao, O.; Nakai, H.; Klene, M.; Li, X.; Knox, J. E.; Hratchian, H. P.; Cross, J. B.; Bakken, V.; Adamo, C.; Jaramillo, J.; Gomperts, R.; Stratmann, R. E.; Yazyev, O.; Austin, A. J.; Cammi, R.; Pomelli, C.; Ochterski, J. W.; Ayala, P. Y.; Morokuma, K.; Voth, G. A.; Salvador, P.; Dannenberg, J. J.; Zakrzewski, V. G.; Dapprich, S.; Daniels, A. D.; Strain, M. C.; Farkas, O.; Malick, D. K.; Rabuck, A. D.; Raghavachari, K.; Foresman, J. B.; Ortiz, J. V.; Cui, Q.; Baboul, A. G.; Clifford, S.; Cioslowski, J.; Stefanov, B. B.; Liu, G.; Liashenko, A.; Piskorz, P.; Komaromi, I.; Martin, R. L.; Fox, D. J.; Keith, T.; Al-Laham, M. A.; Peng, C. Y.; Nanayakkara, A.; Challacombe, M.; Gill, P. M. W.; Johnson, B.; Chen, W.; Wong, M. W.; Gonzalez, C.; Pople, J. A. *Gaussian 03*, revision B.04; Gaussian, Inc.: Pittsburgh, PA, 2004.

(31) Dehu, C.; Meyers, F.; Bredas, J. L. *J. Am. Chem. Soc.* **1993**, *115*, 6198−6206.

(32) Hilger, A.; Gisselbrecht, J. P.; Tykwinski, R. R.; Boudon, C.; Schreiber, M.; Martin, R. E.; Luthi, H. P.; Gross, M.; Diederich, F. *J. Am. Chem. Soc.* **1997**, *119*, 2069−2078.

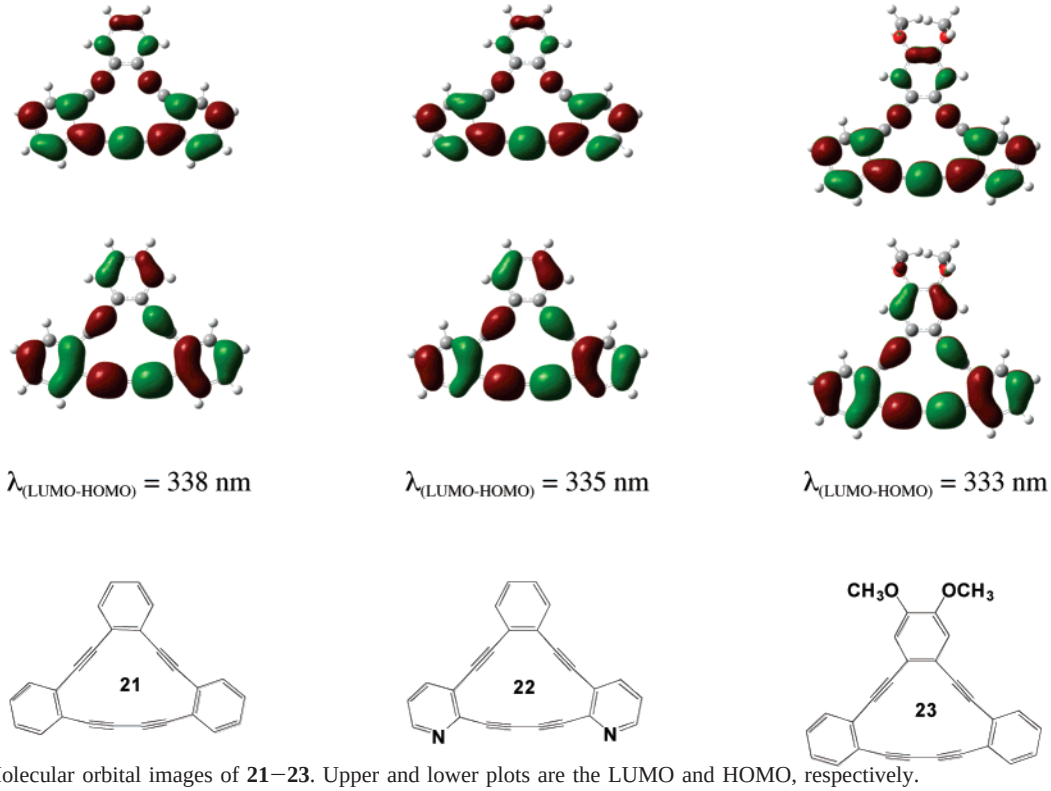

FIGURE 5. Molecular orbital images of **21**−**23**. Upper and lower plots are the LUMO and HOMO, respectively.

The HOMO and LUMO energies were also examined, and calculated optical gaps were compared to the electronic spectra (Table 3). The HOMO−LUMO gaps of **5′**−**7′** are very similar. There is good agreement between the experimental absorption maxima and the wavelengths associated with the calculated optical gaps, suggesting that the first excited states of **5**−**7** are dominated by the HOMO − LUMO transition.

Molecular orbitals for **5′**−**7′** are shown in Figure 4. It is immediately obvious that the HOMOs and LUMOs of **5′**−**7′** contain more π and π* character, respectively, in the pyridine rings than in the donor rings. It is also remarkable that the electron density in each HOMO is delocalized throughout the systems, particularly on the donor ring, while in the LUMO, the electron density is now depleted from the donor ring and localizes along the diacetylene bridge and on the two pyridine rings. This is most noticeable in **5′**, which has the least amount of HOMO electron density on the butadiyne bridge. All LUMOs are strikingly similar. In the HOMO of unsymmetrical **7′**, there is increased electron density along the right-hand side (orientation as shown in Figure 4), but the LUMO of **7′** looks just like the other LUMOs.

The calculated optical gaps and MOs for **5′**−**7′** can be compared to those of the parent hydrocarbon (**21**), the parent dipyridyl system (**22**), and the di-donor compound (**23**). As can be seen in Figure 5, the donor−acceptor modifications change the molecular orbitals very little.

A 5000 step Low Mode−Monte Carlo conformational search [33−35] of the MM2[36] and OPLS2005[37] potential energy surfaces revealed the same lowest energy structures for precursors **13′**, **16′**, and **19′**. These molecules are nonplanar, tweezer-like structures with the untethered terminal acetylenes pointed toward one another approximately 3.9 Å apart. Front and side views of the lowest energy conformer for each system are shown in Figure 6. The precursor molecules are relatively rigid, with 7 to 16 structures found for each ensemble within ∼12 kcal/mol. All lowest energy structures have acetylenes oriented toward one another, while higher energy structures adopt a "W" shape with the acetelynes oriented away from each other on the outside of the molecule. The methoxy orientations increase the ensemble flexibility; the lowest energy structure for **16′** contains *trans*-methoxyl groups; however, **13′** and **19′** adopt less symmetric orientations. Each of the low-energy structures found in the force field study was subjected to a full geometry optimization at the B3LYP/6-31G* level of theory, resulting in very similar structures, confirming the accuracy of the force field results. The density functional results reveal that **19′** is the most stable isomer, while **16′** and **13′** are 1.12 and 2.17 kcal/mol higher in energy (Table 4). The more symmetric **16′** is the least polar. The molecular orbitals reveal π and π* character, respectively, in the pyridine and donor rings in the HOMO and LUMO orbitals, in agreement with the spectroscopic results (vide infra).

TABLE 3. Calculated and Experimental HOMO−LUMO Band Gaps of 5′−7′

	calcd[a]				exptl
	E (HOMO)	*E* (LUMO)	Δ*E* (L−H)	λ (nm)	λ (nm)
5′	−0.214	−0.078	0.136	335	331
6′	−0.211	−0.076	0.135	338	330
7′	−0.212	−0.077	0.135	338	330

[a] Energies are in atomic units (au).

(33) Chang, G.; Guida, W. C.; Still, W. C. *J. Am. Chem. Soc.* **1989**, *111*, 4379−4386.
(34) Kolossvary, I.; Guida, W. C. *J. Am. Chem. Soc.* **1996**, *118*, 5011−5019.
(35) Parish, C.; Lombardi, R.; Sinclair, K.; Smith, E.; Goldberg, A.; Rappleye, M.; Dure, M. *J. Mol. Graphics Model.* **2002**, *21*, 129−150.
(36) Allinger, N. L. *J. Am. Chem. Soc.* **1977**, *99*, 8127−8134.
(37) Kaminski, G. A.; Friesner, R. A.; Tirado-Rives, J.; Jorgensen, W. L. *J. Phys. Chem. B* **2001**, *105*, 6474−6487.

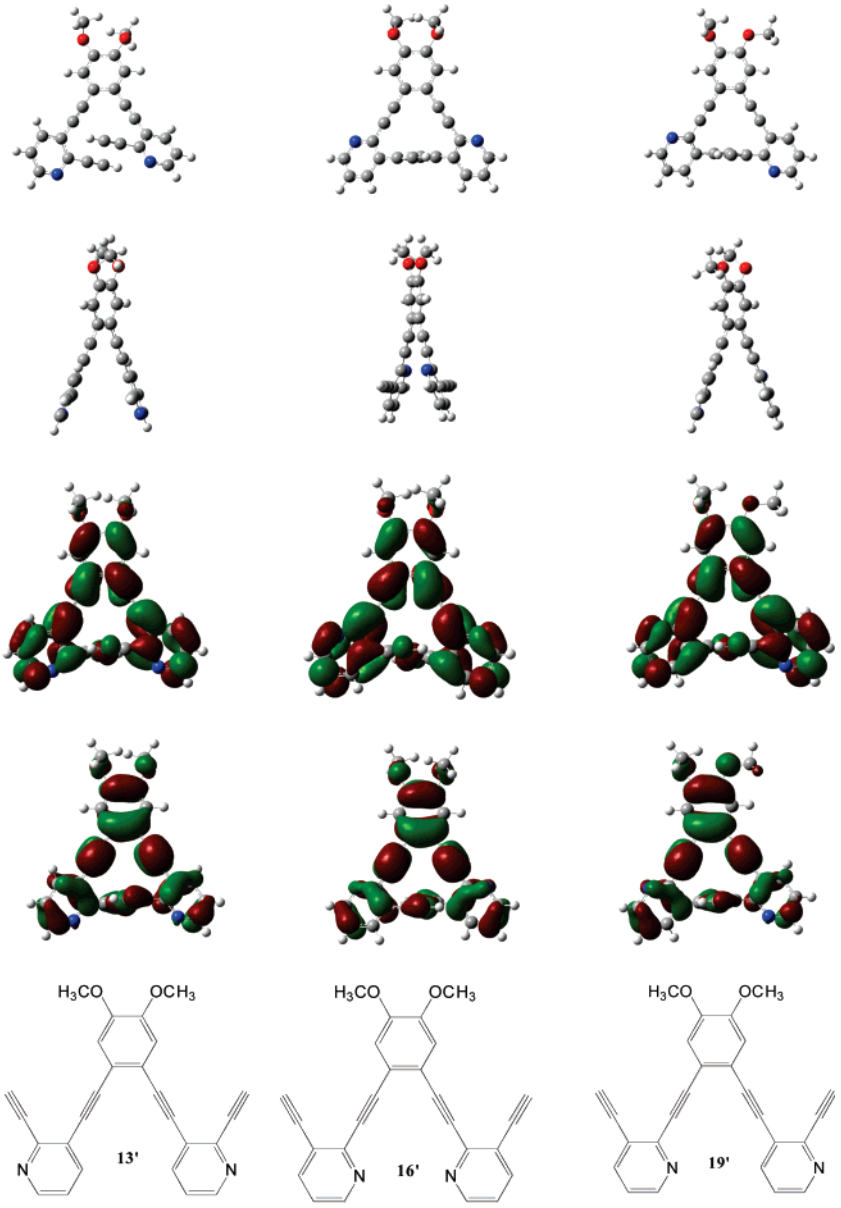

FIGURE 6. Lowest energy conformations (topmost: front view and second column: side view) and molecular orbital images of **13′**, **16′**, and **19′**. Upper and lower MO plots are the LUMO and HOMO, respectively.

TABLE 4. Energetics of 13′, 16′, and 19′ Calculated at the B3LYP/6-31G* Level of Theory

	total energy (au)	ΔE (kcal/mol)	μ (D)
13′	−1260.061 13	2.1700	4.6278
16′	−1260.062 80	1.1175	0.5750
19′	−1260.064 59	0.0000	3.5820

TABLE 5. Calculated and Experimental HOMO−LUMO Band Gaps of 13′, 16′, and 19′

	calcd[a]				exptl
	E (HOMO)	E (LUMO)	ΔE (L−H)	λ (nm)	λ (nm)
13′	−0.209	−0.068	0.141	323	346
16′	−0.207	−0.068	0.139	328	350
19′	−0.202	−0.066	0.136	335	350

[a] Energies are in atomic units (au).

Calculated optical gaps are within 15−23 nm of experimentally measured absorbance peaks and do not correspond to maximum absorbance signals (Table 5). This is likely due to the conformational flexibility present in the precursors that is not available to the cyclized **5′**, **6′**, and **7′**, where agreement between calculated and measured λ_{max} was greater.

Absorption Spectroscopy. The absorption and emission spectra of precursors **13**, **16**, and **19** and of annulenes **5**−**7** are summarized in Table 6. In each absorption spectrum of **13**, **16**, and **19**, three characteristic bands are observed of moderate extinction. The bands are assigned as π,π* transitions and are similar to those observed with other aromatic π conjugated systems. There is little difference between the three spectra, likely due to the available free rotation in the precursor systems.

Like their precursors, the absorption spectra of annulenes **5**−**7** exhibit three major π,π* bands (Table 6). However, each of these complexes exhibits an ca. 50 nm red-shift due to a combination of the forced planarity of the systems and the extended π conjugation available in these molecules. It is

TABLE 6. Absorption and Emission Properties of 13, 16, 19, and 5−7[a]

	absorption		emission
	λ_{max} (nm)	ϵ_{max} (M^{-1} cm^{-1})	λ_{max} (nm)
13	251	51900	411
	303	25700	
	346	15900	
16	251	43000	405
	307	19300	
	350	14200	
19	250	90600	408
	306	51500	
	350	31200	
5	309	62200	457
	321	64700	
	331	66500	
	364	19900	
	402	4500	
6	313	66600	444
	330	104200	
	359	28100	
	384	10000	
7	313	49500	452
	330	61700	
	361	26000	
	407	8600	

[a] All spectra recorded in CH_2Cl_2.

interesting to note the enhanced fine structure observed in **5**, presumably an indication of greater vibronic coupling between the ground and the excited states. While this side band is observed in all three spectra, it has a significantly higher contribution in the spectrum of **5**. The bent conjugation present in **5** is likely responsible for this increased coupling, as the conjugation path is significantly lengthened in comparison to **6**, as suggested by the quinoidal values (vide supra). While the quinoidal values for **6** are less than **5** and **7**, its lowest energy band is not as red-shifted as the other systems. The extended red absorption in **5** and **7** could also be indicative of some extended intermolecular interactions between molecules in the ground state as a result of their higher dipole moments. As expected, the absorption spectrum for **7** exhibits some of the character of both previous spectra, although the fine structure is not pronounced (presumably due to only one side of the system exhibiting the bent charge transfer). While the long wavelength absorption tail observed for **7** might suggest intramolecular charge transfer, this observation is not illustrated in the calculations. The presence of excimer-like aggregates in polyaromatic systems[38] can also produce similar spectra. While absorption concentration studies on **5** and **7** exhibit a linear relationship, a marked negative deviation for **6** is observed, further suggesting aggregation.

Emission Spectroscopy. Emission spectra of precursors **13**, **16**, and **19** and of annulenes **5**−**7** are shown in the Supporting Information and summarized in Table 6. The strong emissions observed from precursors **13**, **16**, and **19** exhibit fluorescence typical of a π,π^* excited state, with an intense primary band along with a vibronic side band red-shifted ca. 20 nm from the primary band. Again, there is little variation between the three spectra, other than a slight blue-shift in the primary band of

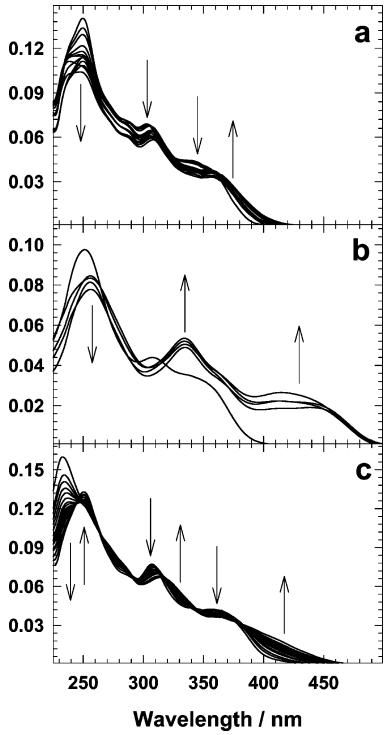

FIGURE 7. Absorption TFA titration of (a) **13**, (b) **16**, and (c) **19**. Spectra were recorded in CH_2Cl_2. Spectra were recorded after sequential aliquot addition of a methanol TFA solution. Absorption intensity trends are indicated by arrows.

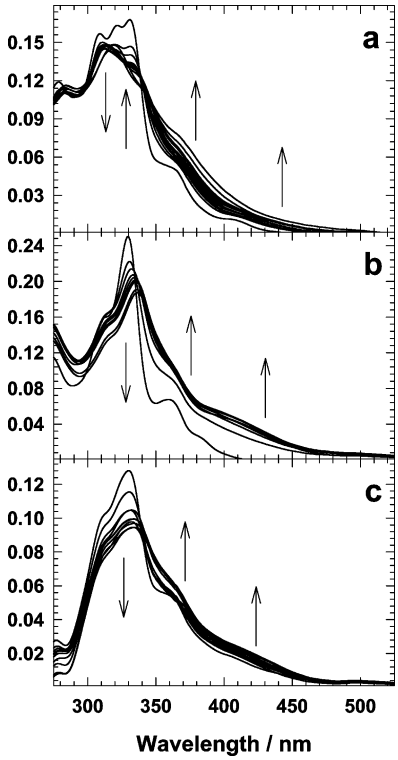

FIGURE 8. Absorption TFA titration of (a) **5**, (b) **6**, and (c) **7**. Spectra are recorded in CH_2Cl_2. Spectra are recorded after sequential aliquot addition of a methanol TFA solution. Absorption intensity trends are indicated by arrows.

(38) Walters, K. A.; Ley, K. D.; Schanze, K. S. *Langmuir* **1999**, *15*, 5676−5680.

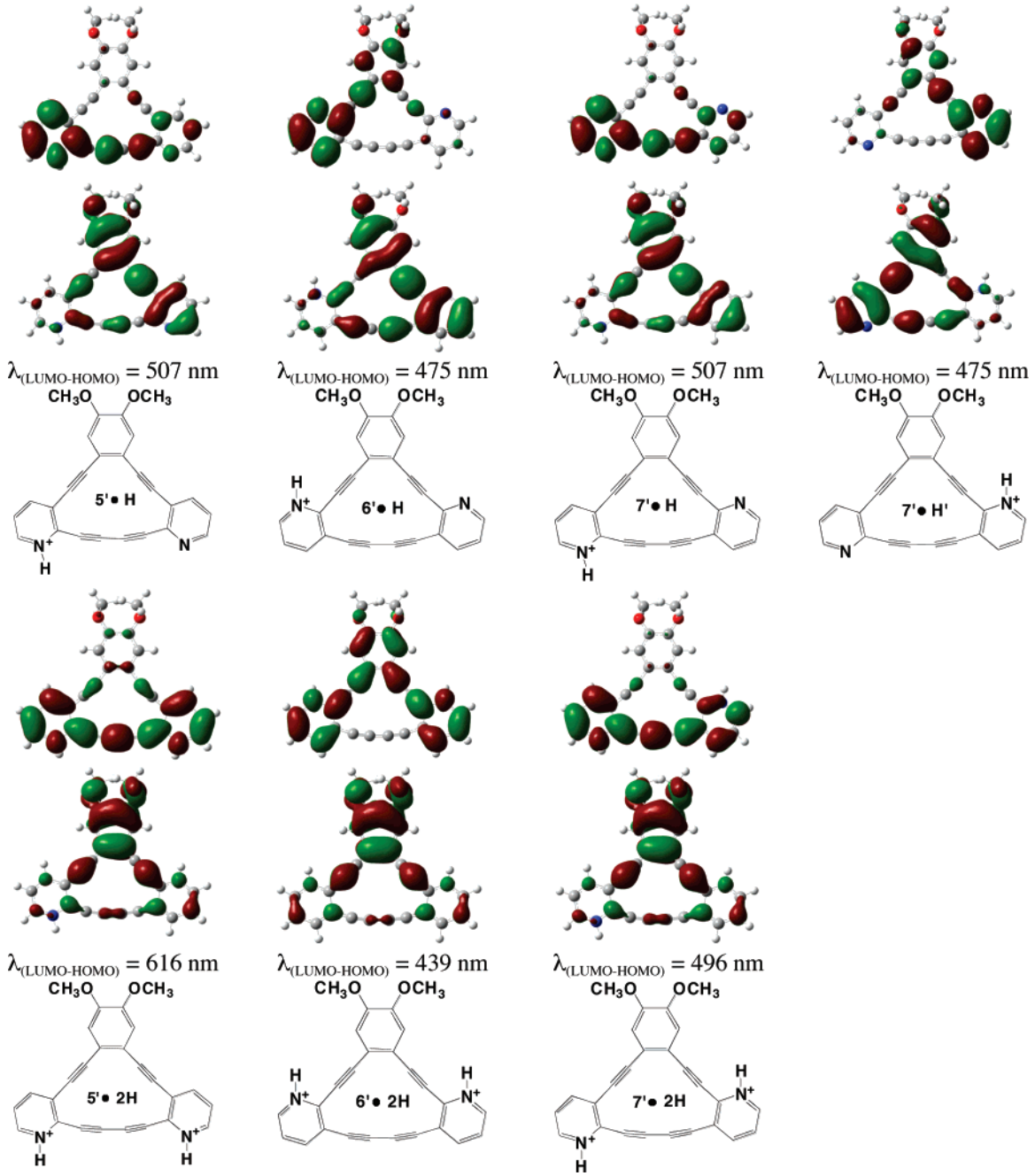

FIGURE 9. Molecular orbital images of mono- and diprotonated forms of **5′**−**7′**. Upper and lower plots are the LUMO and HOMO, respectively.

16. This shift could be indicative of the presence of linear conjugation in this precursor.

Again, a strong fluorescence is observed from annulenes **5**−**7**, typical of a π,π^* excited state, although the vibronic side band is not as prominent. As with the absorption spectra, the emission bands for the final systems are red-shifted ca. 50 nm from their precursors due to the extended conjugation from the forced planarity. Like the absorption spectra, the peak for **6** is ca. 10 nm blue-shifted from the other two systems. The emission spectra, however, are largely uniform, suggesting very similar excited states. This similarity is supported by the LUMO MO calculations for these systems.

TFA Titrations. One application for these systems could be as ion sensors. The protonation of the pyridyl nitrogens in our systems will likely alter their HOMO and LUMO levels and their subsequent spectroscopy. Recent work by other researchers has examined pyridyl protonation through titration with trifluoroacetic acid (TFA) in methanol[39] and CH_2Cl_2[40] to provide a controlled environment to study the spectral changes. Absorption spectra for TFA titrations of precursors **13**, **16**, and **19** and of annulenes **5**−**7** are shown in Figures 7 and 8, respectively. The corresponding emission spectra are provided in the Supporting Information. For each precursor, the absorption spectra decidedly red-shift, but the nature of the new bands differs. The cross-conjugation present in **13** exhibits a single new band at 370 nm, while the linear conjugation in **16** produces two new

(39) Burghardt, S.; Hirsch, A.; Medard, N.; Kachfhe, R. A.; Aussere, D.; Valignat, M. P.; Gallani, J. L. *Langmuir* **2005**, *21*, 7540−7544.

(40) Eckert, J.-F.; Maciejczuk, U.; Guillon, D.; Nierengarten, J.-F. *Chem. Commun.* **2001**, 1278−1279.

bands. Furthermore, the degree of change in **16** is considerably larger than in **13**. While the linear conjugation results in the most stable system (vide supra), the protonated product exhibits a considerable increase in vibronic coupling between the donor and the acceptor moieties that leads to the greatly red-shifted spectrum. The absorption spectra of **17** exhibit the greatest complexity of the three, likely due to the two different pyridyl environments. While some differences exist in the precursor titration spectra, the final systems exhibit remarkably similar spectra. In all cases, the primary band decreases, while two new bands appear slightly red-shifted to the original spectral features. The bent conjugation in **5** retains much of the fine structure previously observed, so protonation does not greatly alter this structural feature. The linear conjugation in **6** leads to more pronounced spectral features, again presumably due to vibronic coupling.

In previous research by Haley and co-workers,[13] different emission spectra are obtained as subsequent pyridyl nitrogens are protonated. Interestingly, our emission spectra do not exhibit multiple signatures suggesting multiple protonations. Instead, the fluorescence is rapidly quenched upon TFA addition and exhibits very little, if any, red-shifting. It is likely that the protonation of the first pyridyl nitrogen alters the MO structure such that an alternate excited state is populated that rapidly decays nonradiatively. Further protonation of the second nitrogen does not significantly alter the excited state manifold such that a radiative decay is again observed. The only red-shifted spectral signature of a protonated form is seen in **16** and **6**, where the linear conjugation pathway again produces stronger coupling. While the 440 nm band does not persist in **16**, even after the addition of 10 molar equiv of TFA, a band at 530 nm persists for **6**.

An examination of the molecular orbitals for the protonated forms of **5′**−**7′** is shown in Figure 9 along with the calculated HOMO−LUMO optical gaps. The mono-protonated forms of **5′**−**7′** show significant charge-transfer transitions from the HOMO to the LUMO. In all three cases, the orbitals in the HOMO are delocalized along one side of the molecule connecting the donor ring with one of the pyridyl rings; in the LUMO, the delocalization shifts to the alternate pyridyl ring with significant diminishment of electron density around the donor ring. The diprotonated systems also exhibit significant charge transfer from the HOMO to the LUMO. In these systems, the HOMO also contains a high level of electron density around the donor ring but with much less density delocalized onto the pyridyl rings/butadiene bridge. In the LUMO of **5′·2H** and **7′·2H**, the density shifts to the opposite side of the molecule encompassing the pyridyl rings and the butadiyne bridge, while in **6′·2H**, the LUMO density is delocalized exclusively over the three rings with no electron density in the butadiyne bridge. The calculated HOMO−LUMO transitions correspond to absorbance peaks (Figure 8) in only one case; the weakest band in the TFA titration of **6** (430 nm) likely corresponds to the calculated HOMO−LUMO optical gap of the diprotonated form at 439 nm. The discrepancy for all other systems likely reflects solvent effects that were not included in the computational results.

Conclusion

We have synthesized three new isomeric dipyridoannulenes in good yields from readily accessible building blocks. The annulenes and their acyclic precursors were analyzed for their optical properties, electronic structure, and behavior in acidic environments. These molecules possess interesting conjugation paths as supported by both spectroscopic and theoretical examination.

The NMR chemical shift differences between the annulenes and the corresponding TIPS-protected precursors support the introduction of new conjugation paths upon cyclization. There is good agreement between the experimental absorption maxima for the dipyridoannulenes and the wavelengths associated with the calculated optical gaps, suggesting that the first excited states are dominated by the HOMO−LUMO transition. Molecular orbital images show that there is charge transfer from the donor ring in the HOMO to the diacetylene bridge in the LUMO of the dipyridoannulenes, while in the acyclic precursors, the charge transfer is less significant. Protonation studies show marked changes in the absorption bands and emission intensities. The linear conjugation lends itself to the greatest spectral changes. These results suggest that the synthesized systems could be utilized in ion sensing applications.

Experimental Section

Compound 13. In a 15 mL pressure tube was placed ca. 13 mL of degassed diisopropylamine, **11** (0.500 g, 1.76 mmol), **12** (0.398 g, 0.84 mmol), $Pd(PPh_3)_2Cl_2$ (0.059 g, 10 mol %, Strem), CuI (0.016 g, 10 mol %), and a stir bar. The solution was bubbled with argon for 3 min and the cap quickly fitted. The tube was placed in an oil bath heated to 80 °C and left for 3 days with stirring. The reaction mixture was concentrated by rotary evaporation at reduced pressure on a 45 °C water bath followed by high vacuum. The crude product was purified by flash chromatography on silica gel eluted with 5−12.5% EtOAc in hexanes. A second purification was carried out using the same procedure giving the product (374 mg, 54%) as a pale brown oil that solidified on prolonged standing in the refrigerator. Mp 77.5−78.5 °C; ^{1}H NMR ($CDCl_3$): δ 8.49 (dd, J = 4.81 Hz, 1.60 Hz, 2H), 7.74 (dd, J = 8.02 Hz, 1.60 Hz, 2H), 7.13 (dd, J = 8.02 Hz, 4.81 Hz, 2H), 6.98 (s, 2H), 4.00 (t, J = 6.87 Hz, 4H), 1.83 (m, 4H), 1.51 (m 4H), 1.11 (m, 42 H), 0.99 (t, J = 7.33 Hz, 6H); ^{13}C NMR ($CDCl_3$) δ 149.5, 148.7, 144.1, 139.7, 123.4, 122.2, 118.8, 115.7, 104.5, 96.0, 95.0, 88.6, 69.0, 31.3, 19.3, 18.8, 13.9, 11.4; IR (KBr) ν 2954, 2939, 2866, 2208, 2159, 1510 cm^{-1}; ESI-HRMS calcd for $C_{50}H_{68}N_2O_2Si_2$: 785.4897 $[M+H]^+$, found: 785.4897.

Compound 14. Into a 500 mL round-bottomed flask was placed 200 mL of THF, **13** (0.358 g, 0.456 mmol), and a stir bar. A septum was fitted, and two needles were inserted. One was connected to an argon line, and a slight flow of argon through the flask was established. The solution was cooled to −78 °C, and with vigorous stirring, TBAF (1.37 mL, 1.37 mmol, 1.0 M in THF) was added dropwise. The solution was stirred for 1 h at −78 °C and then allowed to return to room temperature. Water (25 mL) was added, and the reaction mixture was concentrated by rotary evaporation at reduced pressure on a 45 °C water bath to remove most of the THF. The concentrate was rinsed into a separatory funnel with ca. 80 mL of ether, and the ether solution was washed with water (4 × 50 mL), dried over $MgSO_4$, and rotary evaporated under reduced pressure to give the crude product. The crude product was passed over a short column of silica gel using 10−30% EtOAc in hexanes as the eluent. The product was obtained as a beige solid in 68% yield (146 mg). A ^{1}H NMR spectrum showed the product to be sufficiently pure for use. ^{1}H NMR ($CDCl_3$): δ 8.52 (dd, J = 4.8 Hz, 1.6 Hz, 2H), 7.79 (dd, J = 7.8 Hz, 1.4 Hz, 2H), 7.25 (m, 2H), 7.05 (s, 2H), 4.05 (t, J = 6.4 Hz, 2H), 3.31 (s, 2H), 1.84 (m, 4H), 1.52 (m 4H), 0.99 (t, J = 7.3 Hz, 6H).

Annulene 5. In a 500 mL round-bottomed flask was placed 125 mL of THF and 125 mL of diisopropylamine, both of which had been bubbled with air. Next, $Pd(dppe)Cl_2$ (0.026 g, 15 mol %),

CuI (0.008 g, 15 mol %), I_2 (0.038 g, 50 mol %), and a stir bar were added. A septum was fitted to the flask, and a large needle was inserted to vent the flask to the atmosphere. The flask was placed in an oil bath heated to 60 °C, and the contents were vigorously stirred. To the stirred solution, partially purified **14** (0.140 g, 0.296 mmol, dissolved in 20 mL of THF) was added dropwise over a 20 h period via a syringe pump. The solution was stirred an additional 8 h after the addition was complete. The reaction mixture was concentrated by rotary evaporation at reduced pressure on a 45 °C water bath followed by high vacuum. The crude product was purified by flash chromatography on silica gel eluted with 10−25% EtOAc in hexanes followed by a second column eluted with 10−20% EtOAc in hexanes. The product was obtained as a waxy solid in 40% yield (56 mg). Mp 115.5−116.1 °C; ^{1}H NMR ($CDCl_3$): δ 8.67 (d, J = 4.1 Hz, 2H), 8.19 (d, J = 7.8 Hz, 2H), 7.42 (dd, J = 7.8 Hz, 4.6 Hz, 2H), 7.30 (s, 2H), 4.14 (t, J = 6.4 Hz, 2H), 1.88 (m, 4H), 1.56 (m 4H), 1.03 (t, J = 7.3 Hz, 6H). ^{13}C NMR ($CDCl_3$) δ 149.8, 148.5, 141.4, 139.6, 126.9, 122.7, 119.2, 116.0, 96.9, 89.4, 83.3, 80.3, 69.1, 31.3, 19.3, 14.0; IR (KBr) ν 3040, 2954, 2933, 2872, 2177, 2144,1591, 1516,1412 cm^{-1}; ESI-HRMS calcd for $C_{32}H_{26}N_2O_2$: 493.1892 $[M + Na]^+$, found: 493.1889.

Annulene 6. In a 500 mL round-bottomed flask was placed 125 mL of THF and 125 mL of diisopropylamine, both of which had been bubbled with air. Next, $Pd(dppe)Cl_2$ (0.015 g, 15 mol %), CuI (0.005 g, 15 mol %), I_2 (0.022 g, 50 mol %), and a stir bar were added. A septum was fitted to the flask, and a large needle was inserted to vent the flask to the atmosphere. The flask was placed in an oil bath heated to 60 °C, and the contents were vigorously stirred. Partially purified **17** (83 mg, 0.176 mmol), dissolved in 20 mL of THF, was added dropwise to the stirred solution via a syringe pump over 20 h. The solution was stirred an additional 8 h after the addition was complete. The reaction mixture was concentrated by rotary evaporation at reduced pressure on a 45 °C water bath followed by high vacuum. The crude product was purified by flash chromatography on silica gel eluted with 10−25% EtOAc in hexanes followed by a second column eluted with 10−20% EtOAc in hexanes. The product was obtained as a dark, waxy solid (69 mg, 40% yield). Mp 187.8−188.6 °C (dec); ^{1}H NMR ($CDCl_3$): δ 8.74 (d, J = 4.6 Hz, 2H), 7.90 (dd, J = 7.8 Hz, 1.4 Hz, 2H), 7.48 (s, 2H), 7.33 (dd, J = 8.0 Hz, 4.8 Hz, 2H), 4.11 (t, J = 6.4 Hz, 2H), 1.85 (m, 4H), 1.52 (m 4H), 1.00 (t, J = 7.3 Hz, 6H); ^{13}C NMR ($CDCl_3$) δ 150.1, 149.3, 148.0, 136.8, 121.5, 119.7, 119.5, 115.8, 93.9, 91.5, 93.9, 82.0, 69.2, 31.3, 19.3, 14.0; IR (KBr) ν 2951, 2866, 2180, 1543, 1512, 1424, 1247 cm^{-1}; ESI-HRMS calcd for $C_{32}H_{26}N_2O_2$: 471.2072 $[M + H]^+$, found: 471.2072.

Annulene 7. In a 500 mL round-bottomed flask was placed 125 mL of THF and 125 mL of diisopropylamine, both of which had been bubbled with air. Next, $Pd(dppe)Cl_2$ (0.032 g, 15 mol %), CuI (0.011 g, 15 mol %), I_2 (0.047 g, 50 mol %), and a stir bar were added. A septum was fitted to the flask, and a large needle was inserted to vent the flask to the atmosphere. The flask was placed in an oil bath heated to 60 °C, and the contents were vigorously stirred. To the stirred solution, partially purified **20** (0.175 g, 0.370 mmol) in THF (20 mL) was added dropwise over 20 h via a syringe pump. The solution was stirred an additional 8 h after the addition was complete. The reaction mixture was concentrated by rotary evaporation at reduced pressure on a 45 °C water bath followed by high vacuum. The crude product was purified by flash chromatography on silica gel eluted with 10−25% EtOAc in hexanes followed by a second column eluted with 10−20% EtOAc in hexanes. The product was obtained as a dark, waxy solid (78 mg, 45% yield). Mp 166.8−170.0 °C (dec); ^{1}H NMR ($CDCl_3$): δ 8.75 (d, J = 4.6 Hz, 1H), 8.64 (d, J = 4.6 Hz, 1H), 8.17 (d, J = 7.8 Hz, 1H), 7.94 (d, J = 7.8 Hz, 1H), 7.48 (s, 1H), 7.39 (dd, J = 8.0 Hz, 4.8 Hz, 1H), 7.35 (dd, J = 7.8 Hz, 4.6 Hz, 1H), 7.27 (s, 1H), 4.11 (m, 4H), 1.86 (m, 4H), 1.54 (m 4H), 1.01 (m, 6H); ^{13}C NMR ($CDCl_3$) δ 150.1, 150.0, 149.2, 148.5, 147.8, 141.5, 139.7, 137.2, 126.9, 122.6, 121.6, 119.7, 119.5, 119.2, 116.3, 115.4, 97.0, 9402, 91.2, 89.5, 85.1, 84.0, 81.9, 80.5, 69.2, 69.1, 31.27, 31.26, 19.31, 19.29, 14.0 ($2CH_3$); IR (KBr) ν 2958, 2877, 2181, 1594, 1514, 1426 cm^{-1}; ESI-HRMS calcd for $C_{32}H_{26}N_2O_2$: 493.1892 $[M + Na]^+$, found: 493.1901.

Acknowledgment. This work was supported by awards from the Research Corporation (K.C.R.), the National Science Foundation (CHE-0138640 and CHE-0552292 to K.C.R.), and Northern Kentucky University's Center for Integrated Science and Mathematics (K.C.R. and K.A.W.). K.A.W. acknowledges support from the Camille and Henry Dreyfus Foundation. K.C.R. and C.P. acknowledge support from the National Science Foundation under Grant CHE-0211577. C.P. thanks the Donors of the American Chemical Society Petroleum Research Fund and the Thomas F. and Kate Miller Jeffress Memorial Trust for partial support of this work. C.P. also acknowledges support from the Camille and Henry Dreyfus Foundation through receipt of a Henry Dreyfus Teacher−Scholar award. E.W. acknowledges support from the Arnold and Mabel Beckman Foundation through receipt of a Beckman Scholars award. S.M. thanks CUR. Computational resources were provided, in part, by the MERCURY supercomputer consortium (http://mars.hamilton-.edu) under NSF Grant CHE-0116435.

Supporting Information Available: ^{1}H and ^{13}C NMR spectra for **5**−**7**, **9**, **11**−**13**, **16**, and **19**. Synthesis of **9**−**12** and **15**−**20**. Absorption and emission spectra for **5**−**7**, **13**, **16**, and **19**. Energetics of **5′**−**7′** and Cartesian coordinates for all calculated structures. This information is available free of charge via the Internet at http://pubs.acs.org.

JO7019724